The model designed and meshed in order to import as an input of the software (Li et al., 2019). The tubular shell is 300 mm radios and 700 mm length with 2 mm thickness. Stiffener ring placed in the middle of the shell and welded with eleven pairs of weld lines of 10 mm length and 5 mm leg length. The structure meshed by 38222 tetrahedral elements and 13636 nodes. Figure 4 shows the meshed structure and position of weld lines.

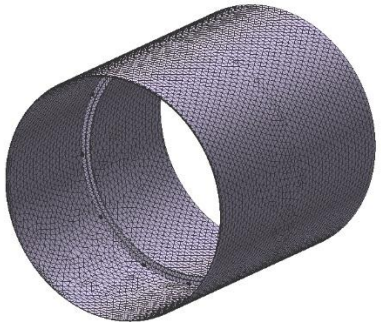

Figure 4: Meshed model for FEM and position of weld lines

The Goldak double ellipsoid model has been used as the heat source. Figure 5 shows the Goldak's ellipsoid model.

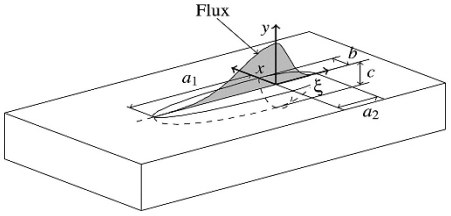

Figure 5: Heat source Goldak's double ellipsoid model (Lorin et al., 2014)

Table 1 shows the dimensions of Goldak's model of the problem.

Table 1: Dimensions' of Goldak's ellipsoid model

a_1	a_2	b	c
3.9	14.3	6	2

Which a_2 is the front length, a_1 is rear length, b is width and c is depth of the heat source.

Heat distribution in front and rear of ellipsoid are:

$$q_f(x,y,z) = \frac{6\sqrt{3} f_f Q}{bca_2\pi\sqrt{\pi}} e^{(-3x^2/b^2)} e^{(-3y^2/c^2)} e^{(-3z^2/a_2^2)} \quad (4)$$

$$q_r(x,y,z) = \frac{6\sqrt{3} f_r Q}{bca_1\pi\sqrt{\pi}} e^{(-3x^2/b^2)} e^{(-3y^2/c^2)} e^{(-3z^2/a_1^2)} \quad (5)$$

Parameters f_f and f_r are factors of temperature distribution that $f_f + f_r = 2$ calculate as:

$$f_f = \frac{2}{1+\frac{a_1}{a_2}} \quad (6)$$

$$f_r = \frac{2}{1+\frac{a_2}{a_1}} \quad (7)$$

Inserted energy distributes as Gaussian mode in any direction through the ellipsoid. Figure 6 shows the peak temperature of welding process of the model in welding simultaneously which raise to 1538°C.

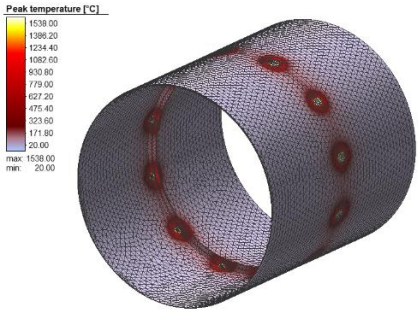

Figure 6: Peak temperature of simultaneous welding both sides of the ring

4. RESULTS AND DISCUSSION

Welding has been simulated on the model in different conditions of welding and effective parameters. The primer current is 210 A, voltage is 25 V, and the speed is 9 cm/min and 0.9 of heat efficiency. The software automatically increased the mesh density beside the weld line simultaneous with the welding process in order to decrease the error rate in heat-affected zone. Welding in the same direction has less residual stress and distortion than welding in opposite directions. Also, separation of the weld line to smaller weld lines reduces these phenomena (Callister and Wiliam, 2000). So, both sides of the ring have been welded in the same direction and separated into eleven weld lines. The welding process has been simulated in different situations by considering welding parameters, preheating and time intervals. Table 2 shows the results of FEM in different conditions. Current has been changed 15% from default measure in some cases and speed has been changed subsequently in a way to keep the net energy per length constant. Time intervals assumed as the time that takes the weld lines of one side of the ring to cool down and then the other side has been welded. In this model, the time interval considered 200 seconds. Residual stresses in main radial directions in different conditions exploited as shown in table 2.

Table 2: Maximum and minimum stresses of considered model in main radial directions and maximum of effective stress.

I [A]	S [Cm/min]	t_i [s]	H [°C]	Tangent (Longitudinal) stress [MPa]		Axial stress [MPa]		Radial stress [MPa]		Effective stress [MPa]
				Max	Min	Max	Min	Max	Min	Max
210	9	–	–	195	-142	420	13	63	-52	364
210	9	200	–	173	-140	390	-2	65	-51	375
210	9	–	150	160	-125	357	10	58	-42	288
241	9	–	–	185	-141	422	9	63	-58	342
178.5	7.6	–	–	199	-149	425	-10	63	-47	345
210	9	200	150	162	-145	380	4	64	-52	315

Where I is current, S is speed, V is voltage, t_i is the interval speed and H is preheating.

According to the results of stresses in main radial directions, the minimum values of tangent stress refer to simultaneous welding with preheating (Max: 162 MPa, Min: -145 MPa), and welding with time interval and preheating (Max: 160 MPa, Min: -125 MPa). Simultaneous welding with preheating (Max: 357 MPa) has the least axial stress. Simultaneous welding (Max: 420 MPa) and simultaneous welding by increasing and decreasing 15% to the current (Max: ~423 MPa) present the highest values of axial residual stress. The contour of the residual stress of simultaneous welding with preheating shown in Figure 7.

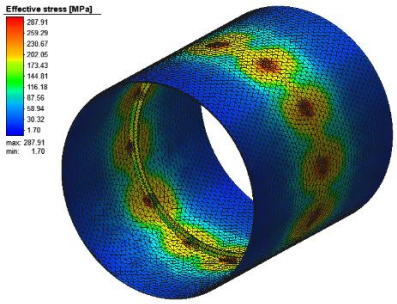

Figure 7: Distribution contour of the effective stress of simultaneous welding with preheating

Maximum distortion of the process in main radial directions and total distortion of the model in considered conditions shown in table 3.

Table 3: Effects of welding and effective parameters on distortion of the model

I [A]	S [cm/Min]	t_i [s]	H [°C]	Max.tangent distortion [mm]	Max axial distortion [mm]	Max.radial distortion [mm]	Max.total distortion [mm]
210	9	–	–	0.59	0.46	0.72	0.77
210	9	200	–	0.35	0.37	0.49	0.61
210	9	–	150	1.06	0.59	1.12	0.57
241.5	10.3	–	–	0.64	0.42	0.72	1.28
178.5	7.6	–	–	0.64	0.46	0.73	0.69
210	9	200	150	0.80	0.58	0.82	0.38

The least tangent (longitudinal) distortion refers to welding simultaneously (Max: 0.59 mm), and welding with the time interval (Max: 0.35 mm). In the axial direction, welding with the time interval (Max: 0.37 mm), and welding by increasing 15% to the current have less distortion (Max: 0.42 mm). Almost, welding by increasing and decreasing 15% to current have almost constant results in all conditions. In the radial direction, distortion results are almost constant in most of the conditions but welding with the time interval (Max: 0.49) has the least distortion among them.

Overall, the total distortion of welding by increasing 15% to the current has the most (Max: 1.28 mm), and simultaneous welding with preheating (Max: 0.57 mm) and welding with time interval and preheating (Max: 0.38 mm) have the least values among considered cases. Distribution contour of total distortion of welding with preheating shown in Figure 8.

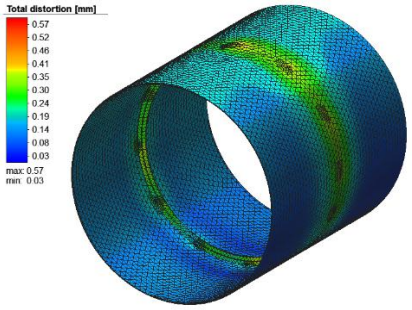

Figure 8: Distribution contour of total distortion of simultaneous welding with preheating

Figure 10 shows the effects of preheating and Figure 11 shows the effects of time interval on effective stress (von Mises stress) of the model which have been exploited from the line of nodes cross two weld lines as shown in Figure 9.

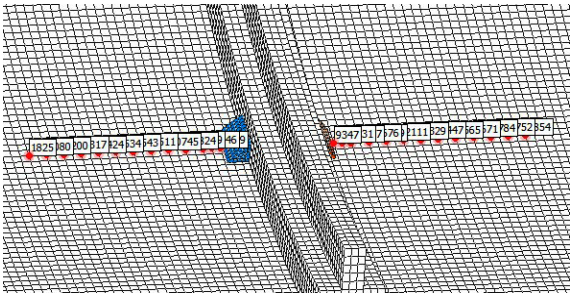

Figure 9: Line of nodes (red dots) considered to exploit plots

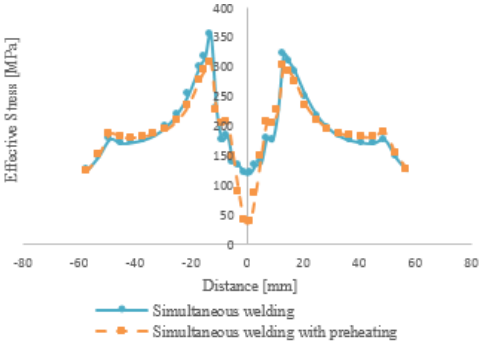

Figure 10: Effects of preheating on effective stress of welding simultaneously.

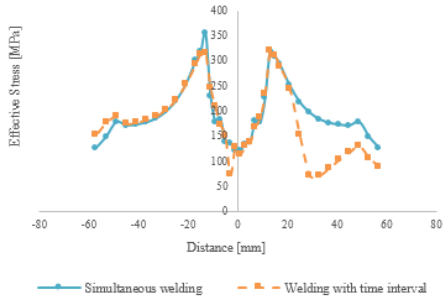

Figure 11: Effects of time interval on effective stress of the model

Current at a specific speed is the most effective parameter in the welding process that controls the fusion rate of the electrode and main parts and has many effects on residual stress and distortion of the model. Figure 12 shows the effects of changing welding current on effective stress.

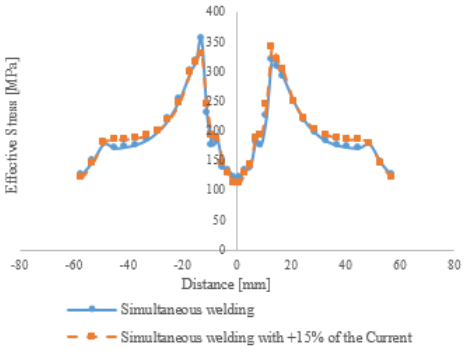

Figure 12: Effects of welding current on effective stress of welding simultaneously

5. CONCLUDING REMARKS

Based on FE analysis of welding the ST52-3N (DIN 1.0570) T-shape stiffener ring in an AISI 4130 (DIN 1.7218) thin-walled tubular shell by eleven pairs of weld lines on both sides of the ring, preheating by making a heat balance and decreasing cooling slope of the parts, reduces plastic deformation and residual stresses. By considering the residual stresses and distortion of different welding conditions in all main radial directions, simultaneous welding with preheating is the best method of welding an ST52-3N (DIN 1.0570) T-shape stiffener ring in an AISI 4130 (DIN 1.7218) thin-walled tubular shell among residual stresses and distortion of considered conditions. Effective stress and total distortion of welding conditions are shown in Figure 13 and Figure 14, respectively.

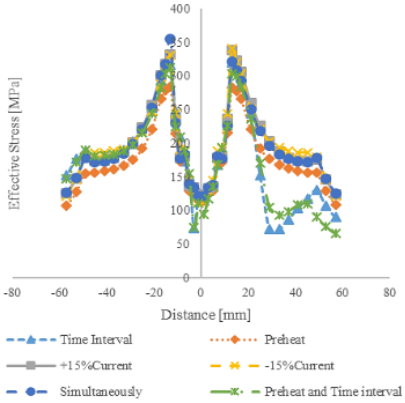

Figure 13: Comparison of effective stresses in considered conditions

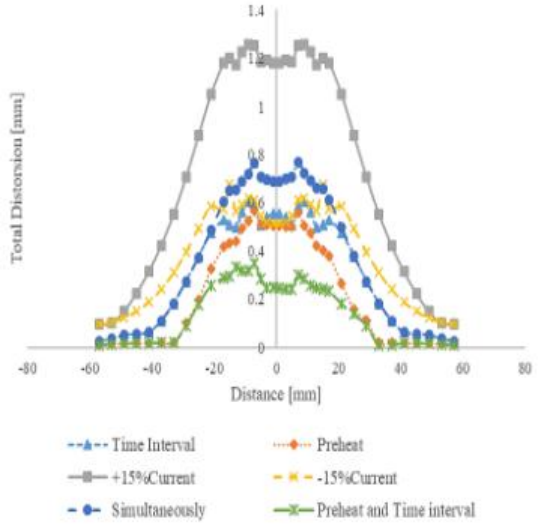

Figure 14: Comparison of total distortion in considered conditions

CONFLICTS OF INTEREST

The authors declare no conflict of interest.

REFERENCES

Barsoum, Z., 2007. Residual Stress Prediction and Relaxation in Welded Tubular Joint. Welding in the World, 51 (1-2), Pp. 23-30.

Callister, William Jr. Materials science and engineering, an introduction. New York: Wiley.

Cerik, B., Cho, S., 2013. Numerical investigation on the ultimate strength of stiffened cylindrical shells considering residual stresses and shakedown. Journal of Marine Science and Technology, 18 (4), pp. 524-534.

Chauhan, V.S., Syed, S.Q., 2015. Numerical Stress Analysis of Uniform and Stiffened Hydraulic Cylinder. International Journal of Scientific Engineering and Research (IJSER), https://www.ijser.in/archives/v3i4/IJSER1580.pdf, 3 (4), 55 – 59.

Deng, D., Murakawa, H., Liang, W., 2007. Numerical simulation of welding distortion in large structures. Computer Methods in Applied Mechanics and Engineering, 196 (45-48), pp. 4613-4627.

Dragi, S., Ivana, V., 2009. Finite element analysis of residual stress in butt welding two similar plates. Scientific Technical Review, 59 (1), pp. 57-60.

Duan, Y., Vincent, Y., Boitout, F., Leblond, J., Bergheau, J., 2007. Prediction of welding residual distortions of large structures using a local/global approach. Journal of Mechanical Science and Technology, 21 (10), pp. 1700-1706.

ER70S-6 - WeldWire", WeldWire, 2019. [Online]. Available: http://www.weldwire.net/weld_products/ww70s-6/. [Accessed: 04-Mar- 2019].

Farkas, J., Jármai, K., Virág, Z., 2004. Optimum Design of a Belt-Conveyor Bridge Constructed as a Welded Ring-Stiffened Cylindrical Shell. Welding in the World, 48 (1-2), pp. 37-41.

Gandhi, P., Raghava, G., Murthy, D., 2000. Fatigue Behavior of Internally Ring-Stiffened Welded Steel Tubular Joints. Journal of Structural Engineering, 126 (7), pp. 809-815. Available: 10.1061/(asce)0733-9445(2000)126:7(809).

Hemmesi, K., Farajian, M., Siegele, D., 2016. Numerical and experimental description of the welding residual stress field in tubular joints for fatigue assessment. Welding in the World, 60 (4), Pp. 741-748.

Lee, C., Chang, K., 2007. Three-dimensional finite element simulation of residual stresses in circumferential welds of steel pipe including pipe diameter effects. Materials Science and Engineering: A, 487 (1-2), Pp. 210-218.

Lee, M., Llewelyn-Parry, A., 1999. Strength of ring-stiffened tubular T-joints in offshore structures. Journal of Constructional Steel Research, 51 (3), Pp. 239-264.

Li, X., Xue, X., Zhang, L., Wang, X., Wang, H., 2019. Experiment and Finite Element Analysis on the Ultimate Strength of Ring-Stiffened Tube-Gusset Joints. International Journal of Steel Structures, 19 (5), Pp. 1534-1542. 2019.

Lorin, S., Cromvik, C., Edelvik, F., Lindkvist, L., Söderberg, R., 2014. Variation Simulation of Welded Assemblies Using a Thermo-Elastic Finite Element Model. Journal of Computing and Information Science in Engineering, 14 (3), Pp. 031003. Available: 10.1115/1.4027346.

Rasti, A., Sattarifar, I., Salehi, M., Karimnia, V., 2014. Stress analysis of welded joints in internal stiffener rings in an aluminum cylinder. Proceedings of the Institution of Mechanical Engineers, Part L: Journal of Materials: Design and Applications, 230 (1), pp. 121-130.

Teng, T., Fung, C., Chang, P., Yang, W., 2001. Analysis of residual stresses and distortions in T-joint fillet welds. International Journal of Pressure Vessels and Piping, 78 (8), pp. 523-538.

Thandavamoorthy, T., Rao, A., Santhakumar, A., 1999. Behavior of Internally Ring-Stiffened Joints of Offshore Platforms. Journal of Structural Engineering, 125 (11), pp. 1348-1352.

Yaghi, A., Hyde, T., Becker, A., Sun, W., Williams, J., 2006. Residual stress simulation in thin and thick-walled stainless-steel pipe welds including pipe diameter effects. International Journal of Pressure Vessels and Piping, 83 (11-12), Pp. 864-874.